

Computational Spectral Imaging Based on Compressive Sensing *

Chao Wang(王超)^{1,2,3}, Xue-Feng Liu(刘雪峰)^{3**}, Wen-Kai Yu(俞文凯)¹, Xu-Ri Yao(姚旭日)³,
Fu Zheng(郑福)³, Qian Dong(董乾)³, Ruo-Ming Lan(蓝若明)⁴, Zhi-Bin Sun(孙志斌)³,
Guang-Jie Zhai(翟光杰)³, Qing Zhao(赵清)¹

¹Center for Quantum Technology Research, School of Physics, Beijing Institute of Technology, Beijing 100081

²China Academy of Engineering Physics, Mianyang 621900

³Key Laboratory of Electronics and Information Technology for Space Systems, National Space Science Center, Chinese Academy of Sciences, Beijing 100190

⁴School of Physics and Electronics, Shandong Normal University, Jinan 250014

(Received 9 August 2017)

Spectral imaging is an important tool for a wide variety of applications. We present a technique for spectral imaging using computational imaging pattern based on compressive sensing (CS). The spectral and spatial information is simultaneously obtained using a fiber spectrometer and the spatial light modulation without mechanical scanning. The method allows high-speed, stable, and sub sampling acquisition of spectral data from specimens. The relationship between sampling rate and image quality is discussed and two CS algorithms are compared.

PACS: 42.30.Wb, 42.30.Va, 42.62.Eh, 42.79.Hp

DOI: 10.1088/0256-307X/34/10/104203

Spectral imaging is a common method in basic and applied scientific research, and is employed in analyzing the special chemical composition and physical structure with microscopy.^[1] Spectral imaging can be generally defined as the combined acquisition of spatial and spectral information. Imaging spectrometers are also mounted airborne and in satellites for remote sensing and astronomical observation.^[2–4] Spectral information can be used in matter analysis in many fields.^[5–7] In biomedical research, an extensive range of applications such as research of protein localization and interactions requires quantitative approaches to analyze several distinct fluorescent molecules at simultaneous time in the same sample.^[8] In fact, these applications are becoming increasingly common with the availability of various fluorescent dyes and proteins with emission ranging from ultraviolet (UV) to far infrared.^[9] Fluorescence spectral imaging technology has, indeed, become a fundamental tool for scientific research.^[10–14]

However, some disadvantages exist in the traditional spectral imaging. In most current spectral imaging technologies, the spatial information is acquired by mechanically scanning the sample point-by-point using a spectrometer. Inevitably, mechanical movement will produce errors in the spatial domain, potentially requiring measurement repeats which waste resources. Additionally, spectral imaging has a remarkable feature of a large amount of data, thus it is often highly compressible.

In digital signal processing area, compressive sensing (CS) has become a popular field since Donoho

published the ‘compressive sensing’ report based on the mathematical theory in the last century.^[11] Since then, in 2008, Candès and Wakin provided an introduction to compressive sampling^[12] and Baraniuk *et al.* developed a new imaging approach using a single-pixel camera based on the theory of CS. This is the first implementation of CS for optical imaging.^[15] Compared with the Shannon–Nyquist sampling theorem, CS provides a sensing framework sampling sparse signals in a more efficient way. The compressed signal is obtained during acquisition with CS, thus avoiding the requirement of digital compression. Since CS requires fewer measurements, it is highly suitable for spectral imaging. A single-pixel camera has also been used in spectral imaging which formerly needed a 2D array detector to obtain the spectral image of an object.^[16–24] Some scientists have compared CS imaging and ghost imaging, and made spectral imaging studies.^[25]

In this work, we focus on fluorescence spectral imaging using a single-pixel camera in which the detector is a spectrometer instead of the traditional 2D array detector. This imaging modality can benefit from CS, since the fluorescence spectral data is typically compressible. The number of measurements is reduced and the imaging process does not require mechanical scanning.

As defined by the Shannon–Nyquist sampling theorem, a limited bandwidth signal can be reconstructed by acquiring the original signal at a rate of at least twice the bandwidth. This provides a theoretical basis for many applications. However, most nature sig-

*Supported by the National Major Scientific Instruments Development Project of China under Grant No 2013YQ030595, the National Natural Science Foundation of China under Grant Nos 11675014, 61601442, 61605218, 61474123 and 61575207, the Science and Technology Innovation Foundation of Chinese Academy of Sciences under Grant No CXJJ-16S047, the National Defense Science and Technology Innovation Foundation of Chinese Academy of Sciences, the Program of International S&T Cooperation under Grant No 2016YFE0131500, and the Advance Research Project under Grant No 30102070101.

**Corresponding author. Email: Liuxuefeng@nssc.ac.cn

© 2017 Chinese Physical Society and IOP Publishing Ltd

nals have a sparse representation in a certain basis. Therefore, we can reconstruct this type of signal with the CS theory beyond the Shannon–Nyquist sampling theorem. Supposing x is the target signal of n dimensions, instead of measuring the target signal itself, we can measure the signal modulated with matrix A ,

$$y = Ax + e, \quad (1)$$

where y is the measurement value with m -dimension, and e is the measurement noise. The matrix A has dimensions of $m \times n$ with $m < n$. Understandably, the equations are fewer than unknowns. Generally speaking, this is an ill-conditioned problem, but we may solve x under some conditions in which A and sparse x are appropriately chosen. The matrix A or a transform of A must obey the restricted isometry property (RIP) restriction, which indicates that the random matrix is proper in almost all situations. The signal x must be sparse or sparse under certain basis such as wavelets and discrete cosine transform (DCT),

$$x = \psi x', \quad (2)$$

where ψ is an $n \times n$ transform matrix, and x' is a sparse vector with n dimension. If x' has k nonzero elements and $k \ll n$, we say that the vector x' is k -sparse. Equation (1) becomes

$$y = A\psi x' + e, \text{ or } \begin{cases} A' = A\psi, \\ y = A'x' + e. \end{cases} \quad (3)$$

We can find an appropriate way to solve Eqs. (2) and (3) by solving the following optimization problem,

$$\min_{x'} \frac{1}{2} \|y - A'x'\|_2^2 + \tau \|x'\|_1, \quad (4)$$

where τ is a parameter weighting the two terms in Eq. (4) which indicates the consistencies of solution with measurement results and prior knowledge of sparse, respectively, and $\|\dots\|_p$ stands for l_p norm, defined as $(\|x\|_p)^p = \sum_{i=1}^N |x_i|^p$. For the vector x' with k -sparse, it can be accurately reconstructed with $q \geq Ck \log(n/k)$ measurements, where n is the element number of x' and C is a constant coefficient.^[11,23] Howland *et al.* gave out a simplified formula, $q \geq 4k \approx n/4$.^[26] In fact, we usually use $n/3$ as an empirical value in the experiment.

Although in theory there are many measurement matrices that can be selected, in many experiments, including ours, only two valued matrices such as ‘0–1’ or ‘–1–1’ can be selected limited by optical components and devices. Most of these matrices obey the Bernoulli distribution. In some specific applications, sparse matrices can also be used, with only a small number of ‘1’ in the matrix.

A typical spectral imaging data is a three-dimensional digital array which is organized in the data cube.^[20] As shown in Fig. 1, (x, y) represents the

spatial information, and λ represents the spectral information. In this data cube, a fixed λ determines the spatial image and a fixed (x, y) determines the spectral sequence.

In traditional methods, we would obtain the data cube through mechanically scanning each spatial point with a spectrometer, which is prone to error and is labor-intensive. Therefore, we developed a compressive fluorescence spectral imaging (CFSI) system for measuring in spatial and spectral domains at the same time without mechanical scanning.

With the ‘0–1’ random matrix which obeys the Bernoulli distribution loaded on the digital micro-mirror device (DMD), usually the random matrix is about 50% ‘1’ and 50% ‘0’. Therefore, our system can collect about 50% light energy from the object to the detector per measurement. The CFSI system is shown in Fig. 2.

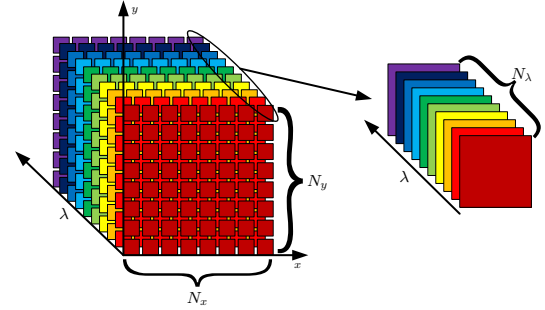


Fig. 1. Spectral imaging data cube.

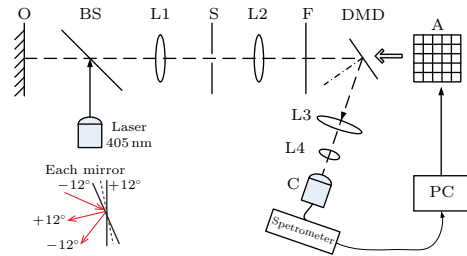


Fig. 2. CFSI system.

With the 405 nm laser source exciting an object, the fluorescent image is projected onto the DMD through two lenses, L1 and L2. To simplify the reconstruction, we make a microscopic image of the object on a small part of the DMD. The image has a size of about $1 \times 1 \text{ mm}^2$ and occupies 64×64 pixels. The whole DMD consists of 1024×768 micro-mirrors, which independently reflect the light to two directions ‘0’ and ‘1’, according to the ‘0–1’ random matrix loaded on the DMD, where ‘0’ and ‘1’ present at -12° and $+12^\circ$ of the micro-mirrors, respectively. Here O is the object prepared with fluorescent materials, and S is a slit, used to adjust the luminous flux and block stray light. The long wave pass filter F blocks the 405 nm laser in the imaging light path. Lenses L3 and L4 are placed in the ‘1’ direction, collecting light from parts of the image with position coordinates cor-

responding to '1' in the matrix to the fiber collimator C. The light is then transferred by the fiber to a spectrometer to measure the spectra. In the experiment, N random matrix A will be loaded on the DMD, making different parts of the object be collected, and N correspondent spectra lines y are given by the spectrometer. The random matrix A and spectra y make up a linear equation as

$$y(\lambda) = A(x)t(x, \lambda), \quad (5)$$

where $t(x, \lambda)$ is the transmission function of object under different wavelengths λ , and x is the two-dimensional coordinate of the image on the DMD. Measurement matrix A is independent of λ as the reflection of the DMD is uniform for every wavelength within the working range of 400–760 nm. Therefore, with intensities of each wavelength in the spectra lines and corresponding measurement matrix, the object of different wavelengths can be imaged respectively.

In the experiment we used a commercial spectrometer (ULS3648, AVANTES) with spectral range of 200–1100 nm, spectral resolution of 1.4 nm and minimum integral time of 10 μ s. The flip frequency of DMD (Discovery 4100, TI) can reach 32 kHz theoretically but we use 100 Hz in the experiment limited by the illumination intensity. Firstly, we measured the fluorescence spectra of two types of materials which comprise the object, as shown in Figs. 3(a) and 3(b), respectively. The spectral peak of light purple material is at 468 nm and the pink material at 636 nm. We made an object with the shape of N, as shown in Fig. 4. The image on the DMD occupies 64×64 pixels, which is therefore the resolution of the final imaging result. To obtain the spectral images, 2468 random matrices were used to drive the DMD, and the spectrometer made a measurement during each state of DMD. Finally, we obtained the data shown in Fig. 5. The spectrometer outputs 2468 sets of spectral data with the DMD flipping 2468 times and the elapsed time is 24.68 s. The spectra shown in Figs. 3(a) and 3(b) of light purple and pink materials were measured by the spectrometer mentioned in Fig. 2. According to the peak values of the spectrums, we reconstructed the image depending on CS using the vertical data at 468 nm and 636 nm. The CS algorithm we used is a total variation augmented Lagrangian alternating direction algorithm (TVAL3) used to calculate the sparsest solution in gradient domain under '0–1' random measurement matrix. Figure 6(a) is the reconstructed image at 468 nm and Fig. 6(b) at 636 nm. We add the pixel values of the two images in Figs. 6(a) and 6(b) together as the fusion image, as shown in Fig. 6(c). As a comparison, we also use the orthogonal matching pursuit (OMP) algorithm to reconstruct the image based on spatial sparsity. Figure 7(a) is the reconstructed image at 468 nm and Fig. 7(b) at 636 nm. Figure 7(c) is the fusion image. Obviously, the image quality of Fig. 6 is better than Fig. 7 for the different algorithms. Since most of the common im-

ages are sparse in the gradient domain, the TVAL3 algorithm is more suitable for image reconstruction. Regardless of the TVAL3 algorithm or the OMP algorithm, it takes about 1–2 s to reconstruct a 64×64 image if running on the common computer.

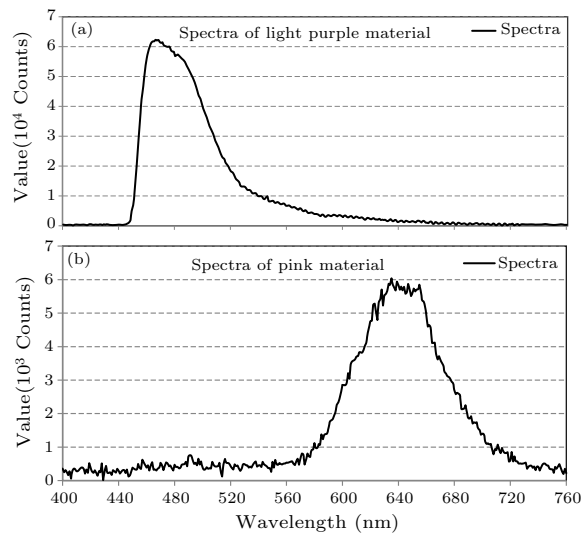


Fig. 3. (a) Spectra of light purple material, and (b) spectra of pink material.

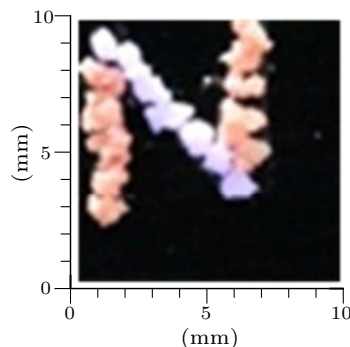


Fig. 4. The object N composed of the fluorescent materials.

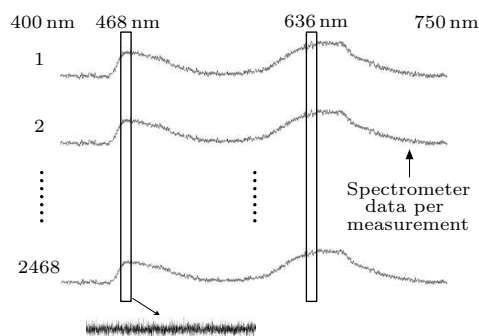


Fig. 5. The measurement data and application data (only in the visible spectrum).

Indeed, image under every wavelength can be obtained respectively based on the data in our experiment. The spatial and spectral information is measured simultaneously. As the two-dimensional spatial information can be obtained with point measurement

based on CS, scanning in neither spatial nor spectral dimensions is required. Moreover, the sampling number can be much less than the image pixels, reducing the measurement time compared with traditional spatial scanning, in which the spectrum measurement must be implemented for every single pixel. Therefore, our experiment provides a stable high-effective scheme of spectral imaging.

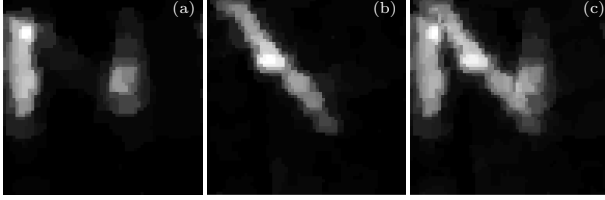


Fig. 6. Spectral imaging result of the fluorescent materials with TVAL3: (a) 468 nm, (b) 636 nm and (c) fusion image.

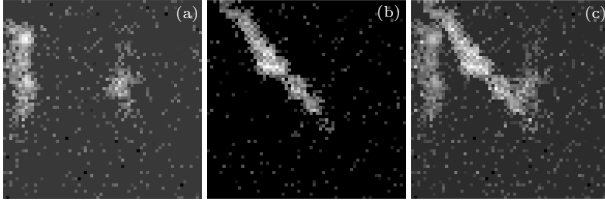


Fig. 7. Spectral imaging result of the fluorescent materials with OMP: (a) 468 nm, (b) 636 nm and (c) fusion image.

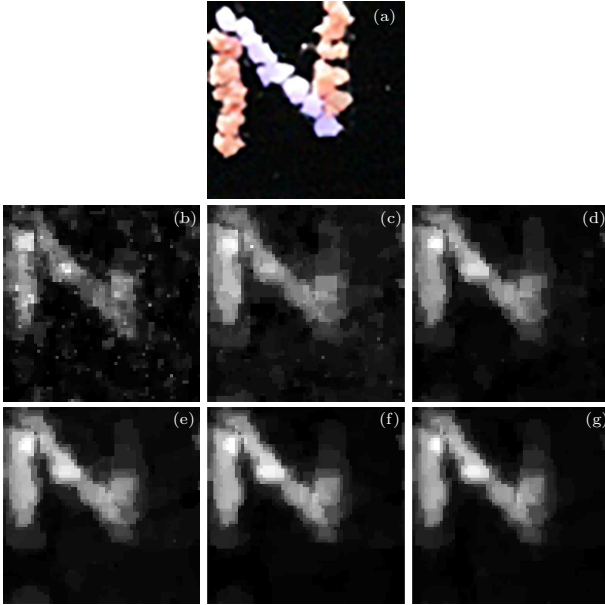


Fig. 8. The image quality with different sampling rates (TVAL3): (a) CCD image, (b) 10%, (c) 20%, (d) 30%, (e) 40%, (f) 50% and (g) 60%.

In the CFSI system, we obtain the image with a size of 64×64 pixels with the measurement value of 2468, and the sampling rate is about 60%. Usually, the CS algorithm has a feature that high sampling rate results in image of high quality. Figure 8(a) is the CCD image, and Figs. 8(b)–8(g) are the fluores-

cent material images with 10%, 20%, 30%, 40%, 50% and 60% sampling rates reconstructed by the CFSI system using TVAL3.

Because the image always contains certain structural information and there is correlation between pixels, we evaluate the image using the structural similarity index measurement (SSIM) which scales the distortion of structure information by brightness, contrast, and structure. The original image and the reconstructed image are divided into average blocks. The total number of blocks is B , whereas b and b' represent the blocks in the original image and the reconstructed image, respectively. The SSIM can be calculated as

$$\text{SSIM}(b, b') = l(b, b')^\alpha \cdot c(b, b')^\beta \cdot s(b, b')^\gamma, \quad (6)$$

and $l(b, b') = \frac{2\mu_b\mu_{b'} + C_1}{\mu_b^2 + \mu_{b'}^2 + C_1}$, $c(b, b') = \frac{2\sigma_b\sigma_{b'} + C_2}{\sigma_b^2 + \sigma_{b'}^2 + C_2}$, $s(b, b') = \frac{\sigma_{bb'} + C_3}{\sigma_b\sigma_{b'} + C_3}$, where α , β and γ are the weights of brightness, contrast and structure, respectively, μ_b , $\mu_{b'}$, σ_b^2 , $\sigma_{b'}^2$, $\sigma_b\sigma_{b'}$ are the means, variances and covariances of b and b' , $l(b, b')$, $c(b, b')$, $s(b, b')$ are the comparison function of brightness, contrast and structure, respectively. Finally, the mean SSIM (MSSIM) can be calculated by^[27]

$$\text{MSSIM}(x, x') = \frac{1}{B} \sum_{j=1}^B \text{SSIM}(b_j, b'_j). \quad (7)$$

The result of MSSIM is shown in Fig. 9 and $\alpha = \beta = \gamma = 1$. If the sampling rate is less than 30%, the quality of the reconstructed image is very poor. However, if the rate is more than 30%, the image quality will be significantly improved. Indeed, we can easily find that the image quality rises slowly at the sampling rates 30%–60% from Fig. 9. We know that higher sampling rate means more sampling time in the experiment. Therefore, in consideration of the practical application based on the compromise strategy, it is recommended to use the sampling rate of just over 30%.

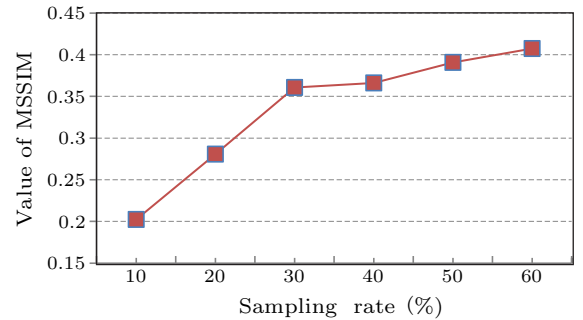


Fig. 9. Image quality assessment with MSSIM.

Finally, we compare CS imaging and CCD images to discuss imaging quality problems. Theoretically, the quality of CS reconstructed images and CCD images should be comparable. However, in Fig. 8, the image of CCD looks better than the CS reconstruction image. There are several possible reasons. The

first is the signal to noise ratio of the detector, the second is the resolution of the detector, the third is the stability of the light source, and the fourth is the light path noise. This is also the focus of our future research on improving image quality.

In summary, we have demonstrated the spectral and spatial imaging method with a spectrometer without any mechanical scanning in the CFSI system. With the DMD modulation providing the spatial resolution, we can obtain spectral images within the wavelength range of the spectrometer simultaneously. The spectral resolution depends on the optical system and the spectrometer. Although the quality of image is not perfect, it is possibly improved with the development of CS algorithm. Our method provides a stable high-speed scheme of fluorescence spectral imaging, which is anticipated to be useful in biomedicine, astronomy, material science, and other related fields.

References

- [1] Studer V, Bobin J, Chahid M, Mousavi H S, Candes E and Dahan M 2012 *Proc. Natl. Acad. Sci. USA* **109** 1679
- [2] Green R O, Eastwood M L, Sarture C M, Chrien T G, Aronsson M, Chippendale B J, Faust J A, Pavri B E, Chovit C J, Solis M, Olah M R and Williams O 1998 *Remote Sens. Environ.* **65** 227
- [3] King M D, Kaufman Y J, Menzel W P and Tanre D 1992 *IEEE Trans. Geosci. Remote Sens.* **30** 2
- [4] Poglitsch A, Waelkens C, Bauer O H, Cepa J, Feuchtgruber H, Henning T, Van Hoof C, Kerschbaum F, Krause O, Renotte E, Rodriguez L, Saraceno P and Vandenbussche B 2008 *Proc. SPIE* **7010**
- [5] Nallala J, Gobinet C, Diebold M D, Untereiner V, Bouche O, Manfait M, Sockalingum G D and Piot O 2012 *J. Biomed. Opt.* **17** 116013
- [6] Bar-Ilan Y and Yelin D 2014 *Opt. Lett.* **39** 5177
- [7] Naik D N, Pedrini G, Takeda M and Osten W 2014 *Opt. Lett.* **39** 1857
- [8] Zimmermann T, Rietdorf J and Pepperkok R 2003 *FEBS Lett.* **546** 87
- [9] Giepmans B N, Adams S R, Ellisman M H and Tsien R Y 2006 *Science* **312** 217
- [10] Deloye C J, Flake J C, Kittle D, Bosch E H, Rand R S and Brady D J 2013 *Excursions in Harmonic Analysis* (Boston: Birkhäuser) vol 1 p 151
- [11] Donoho D L 2006 *IEEE Trans. Inf. Theory* **52** 1289
- [12] Candès E J and Wakin M B 2008 *IEEE Signal Process. Mag.* **25** 21
- [13] Yue X L, Ma F and Dai Z F 2014 *Chin. Phys. B* **23** 044301
- [14] Xue H B, Wang X J, Feng Y Y, Zhu C X, Ye X Y and Zhou Z Y 2009 *Chin. Phys. B* **18** 03373
- [15] Duarte M F, Davenport M A, Takhar D, Laska J N, Sun T, Kelly K F and Baraniuk R G 2008 *IEEE Signal Process. Mag.* **25** 83
- [16] Arguello H and Arce G 2010 *Eur. Signal Process. Conf. (Aalborg Denmark 23–27 August 2010)* p 1434
- [17] Arguello H and Arce G 2011 *J. Opt. Soc. Am. A* **28** 2400
- [18] Arce G R, Brady D J, Carin L, Arguello H and Kittle D S 2014 *IEEE Signal Process. Mag.* **31** 105
- [19] Fu C, Arguello H, Sadler B M and Arce G R 2015 *J. Opt. Soc. Am. A* **32** 2178
- [20] August Y, Vachman C, Rivenson Y and Stern A 2013 *Appl. Opt.* **52** D46
- [21] Rivenson Y and Stern A 2009 *IEEE Signal Process. Lett.* **16** 449
- [22] Yu W K, Liu X F, Yao X R, Wang C, Zhai G J and Zhao Q 2014 *Phys. Lett. A* **378** 3406
- [23] Candès E J and Tao T 2006 *IEEE Trans. Inf. Theory* **52** 5406
- [24] Qian L L, Lü Q B, Huang M and Xiang L B 2015 *Chin. Phys. B* **24** 080703
- [25] Lu M H, Shen X and Han S S 2011 *Acta Opt. Sin.* **31** 98 (in Chinese)
- [26] Howland G A, Dixon P B and Howell J C 2011 *Appl. Opt.* **50** 5917
- [27] Wang Z, Bovik A C, Sheikh H R and Simoncelli E P 2004 *IEEE Trans. Image Process.* **13** 600